Investigation of the indium effect on the structural, optical and wettability characteristics of SnO_2 thin films prepared by rapid thermal evaporation

L. Baghriche[a,*], D. Dergham[b,*], F. Lekoui[b], K. Badani[c], S. Hassani[b], D. Guitoume[d], A. Ayadi[e], and F. Ynineb[f]

[a]*Ecole Nationale supérieure d'hydraulique (ENSH), 29 route de, Soumaâ, Algérie,*
[*]*e-mail: l.baghriche@ENSH.dz*
[b]*Division Milieux Ionisés & Laser, Centre de Développement des Technologies Avancées, Cité 20 Août 1956, Baba Hassen, Alger, Algeria,*
[*]*e-mail: ddergham@CDTA.dz*
[c]*Département des sciences de la matière, Université Ben Youcef Ben Khedda Alger Algérie,*
[d]*Research Unit in Optics and Photonics (UROP-CDTA), El Bez, Sétif1 University, Sétif, Algeria,*
[e]*Laboratory of Microstructure and Defects in Materials, Department of Physics, University of Constantine 1, Frères Mentouri, Constantine, Algeria,*
[f]*Research Center on Semiconductors Technology for Energetic (CRTSE) Algiers Algeria.*

Received 24 November 2025; accepted 14 January 2026

While indium (In) doping of tin oxide (SnO_2) has been extensively explored for its structural, optical, and electrical properties, its combined effect on surface wettability and multifunctional performance remains largely unexplored. In this study, indium-doped SnO_2 thin films were synthesized via rapid thermal evaporation, and their structural, morphological, optical, electrical, and wettability properties were systematically correlated.

Both undoped and In-doped films were deposited on glass and silicon substrates. X-ray diffraction (XRD) confirmed the formation of polycrystalline SnO_2 with a dominant tetragonal phase in both undoped and doped samples, while atomic force microscopy (AFM) revealed a significant reduction in surface roughness from 9.6 nm for undoped films to 3.6 nm upon incorporation of 5 wt.% indium. Optical transmission measurements, carried out using a UV-Vis spectrophotometer showed enhanced optical transparency with indium incorporation, reaching over 86% at 5 wt.% In and remaining around 80% for higher doping levels (10-15 wt.%).

The optical band gap exhibited minor variations with doping, initially increasing from 3.80 eV (undoped) to 3.81 eV (5 wt. %), then slightly decreasing to 3.78 eV (10 wt. %), and rising again at 15 wt. % indium, reflecting tunable optoelectronic behavior.

Four-point probe measurements demonstrated a decrease in resistivity with increasing indium content. Contact angle measurements using a surface tensiometer showed that all films displayed hydrophilic surfaces.

Keywords: SnO_2-In thin films; rapid thermal evaporation; XRD; optical properties; hydrophilicity.

DOI: https://doi.org/10.31349/RevMexFis.72.031003

1. Introduction

Transparent conducting oxides (TCOs) are a class of materials that possess a unique combination of high optical transmittance in the visible range and appreciable electrical conductivity, making them indispensable in various optoelectronic and photonic applications. These include flat-panel displays, smart windows, solar cells, touchscreens, light-emitting diodes (LEDs), and sensor technologies [1, 2]. Among the numerous TCO candidates, tin dioxide (SnO_2) has attracted significant attention due to its wide band gap (3.6 eV), chemical stability, low cost, and compatibility with a variety of deposition methods [3, 4]. As an n-type semiconductor, the electrical conductivity of SnO_2 is primarily attributed to intrinsic point defects such as oxygen vacancies and tin interstitials, which act as electron donors [5]. To enhance the performance of SnO_2 films for targeted applications, doping strategies have been widely explored. The incorporation of aliovalent dopants into the SnO_2 lattice can effectively tailor its electrical, structural, and optical characteristics by modifying the carrier concentration, defect chemistry, and crystallinity [6]. Among the potential dopants, indium (In) is particularly promising due to its similar ionic radius to Sn^{4+}, which facilitates substitution in the SnO_2 lattice, potentially improving film conductivity and modifying optical band structures without significantly compromising transparency [7, 8]. In-doped SnO_2 is well known for its excellent optoelectronic properties, but moderate doping levels can offer additional benefits such as improved surface quality, tunable wettability, and reduced grain boundary scattering [9]. In addition to electrical and optical characteristics, the surface wettability of TCO films has gained increasing attention in recent years, especially for applications involving antifogging coatings, and microfluidic devices [10,11]. Thus, understanding the interplay between doping and surface behavior is essential for optimizing TCOs for multifunctional applications [12]. Various physical and chemical deposition techniques have been employed to synthesize In-doped SnO_2 thin films, including spray pyrolysis, sol-gel, sputtering, and

pulsed laser deposition [13, 14]. However, rapid thermal evaporation (RTE) emerges as a cost-effective and scalable method, capable of producing high-purity films with controlled stoichiometry and thickness. Despite its advantages, studies on the influence of indium doping on SnO_2 films fabricated via RTE remain limited in the literature. In this work, we aim to investigate the effects of indium incorporation on the structural, optical, and wettability properties of SnO_2 thin films deposited by rapid thermal evaporation. Structural analysis was performed using X-ray diffraction (XRD) to examine phase composition and crystallinity. Surface morphology and roughness were evaluated using atomic force microscopy (AFM), while UV-Vis spectroscopy was employed to study the optical transmittance and estimate the optical band gap. Electrical resistivity was measured using the four-point probe method, and contact angle measurements were carried out to assess the films' hydrophilicity. The results are expected to provide insights into the tunability of SnO_2 properties through indium doping and highlight the potential of RTE as a viable deposition technique for functional oxide coatings.

2. Experimental method

Thin films of pure SnO_2 and indium-doped SnO_2 with different concentrations (5wt. %, 10wt. %, 15wt. %) were deposited on glass and silicon substrates using a vacuum thermal evaporation process, the evaporation device is a homemade equipment. SnO_2 and In powders have been purchased from Sigma-Aldrich with 99.99% of purity. Prior to deposition, the substrates were ultrasonically cleaned, then placed in a vacuum chamber, which was evacuated to a pressure $\sim 10^{-6}$ mbar. A high voltage was applied across the crucible to have $\sim 1600°\mathrm{C}$ and evaporate the mixed powders rapidly with a deposition time of 15 s. After deposition, the samples were annealed in air at $500°\mathrm{C}$ for 1 hour. The deposited and annealed films were characterized using several techniques. The surface morphology and crystal structure of the thin films were analyzed using Atomic Force Microscopy (AFM) (Nanosurf Flex-AFM system), with AFM images obtained at a resolution of 256×256 pixels over scanning areas of 5×5 μm. Image processing and surface roughness calculations were carried out using Gwyddion software. X-ray diffraction (XRD) analysis was conducted using a Bruker D8 Advance instrument (Germany) with a $CuK\alpha$ cathode source (wavelength = 1.54 Å). The crystal structure data was collected in step-scan mode within a 2θ range of 20^o to 80^o. The optical transmittance of the deposited films was measured using a SHIMADZU UV-1601 ultraviolet-visible spectrophotometer. The sheet resistance was calculated using Keithley's 2400C four-probe method. Photoluminescence spectra were recorded under 325 nm excitation using a Perkin-Elmer LS50B luminescence spectrometer at the Research Center in Semiconductor Technology for Energy. The measurements were carried out at a scan rate of 300 nm/min and at room temperature. The water contact angles of the films measurements were determined by GBX "Digidrop" optical contact angle measurer instrument.

3. Results and discussion

Figure 1 illustrates the diffraction patterns obtained for the pure SnO_2 film and for SnO_2 films doped with indium concentrations ranging from 5 wt.% to 15 wt.%. All samples reveal well-defined polycrystalline features with clear texturing, indicating that crystal growth occurs preferentially along certain directions. In the undoped film, the peaks detected at $26.54°$, $38.94°$, and $57.97°$ are attributed to the (110), (111), and (002) planes of tetragonal SnO_2, in agreement with the reference data provided by JCPDS card No. 41-1445.

The introduction of 5 wt.% indium leads to the appearance of additional diffraction peaks at $26.61°$, $33.77°$, $37.74°$, $42.66°$, $51.93°$, and $58.00°$, indexed to the (110), (101), (200), (210), (211), and (002) orientations, respectively. A marked intensification of the dominant (110) reflection at $26.61°$ is observed without any peak shift, indicating enhanced crystallization and/or expansion of grain dimensions. Such behavior is typically linked to the dopant's capacity to inhibit the formation of new nuclei at low concentrations [15]. The (110) plane remains the preferred growth direction for both the undoped and the 5 wt.% In-doped films, a characteristic known to be advantageous for sensing applications due to its structural robustness and efficient interaction with adsorbed oxygen species [16].

Crystallite size was estimated using Scherrer's equation, which is commonly used by researchers for the evaluation of nanoscale grain dimensions [17].

$$\frac{0.9}{\beta \cos(\theta)}, \tag{1}$$

where D is the grain size, is the wavelength of X-Ray ($=$ 1.54 Å), θ is the Bragg angle and the full width at half maximum (FWHM) after removing the instrumental broadening,

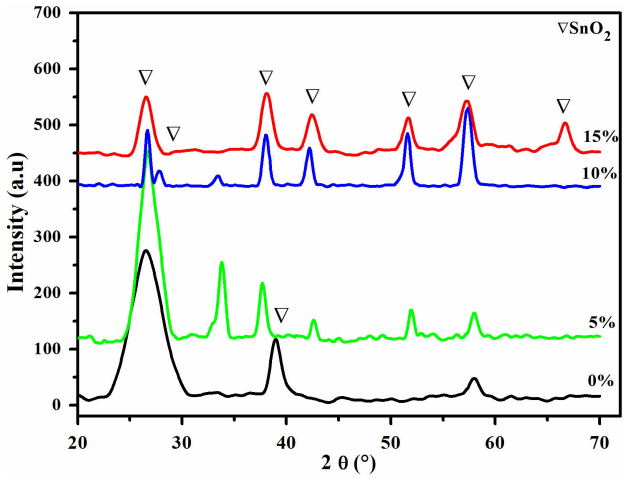

FIGURE 1. XRD patterns for the undoped and In-doped SnO_2 layers (JCPDS card No. 41-1445).

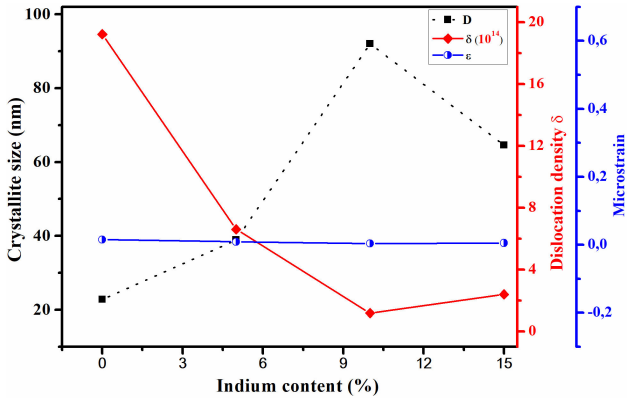

FIGURE 2. Variation of crystallite size, Dislocation density and microstrain as a function of In content.

$$\beta = \sqrt{\beta^2_{FWHM} - \beta^2_0},$$

β_{FWHM} is the full width at half maximum and β_0 is the correction factor (0.007 radians). The grain size values are listed in Table I. Figure 2 illustrates how these values vary with doping concentration.

The undoped sample exhibits a grain size of 22.8 nm. Upon introducing 5 wt. % and 10 wt. % In into the SnO_2 structure, the crystallite size increases to 38.9 nm and 92 nm, respectively. This enhancement can be attributed to improved adatom diffusion between adjacent crystallites due to doping, which promotes coalescence and consequently increases grain size. However, at 15 wt. % In doping, the grain size decreases to 64.6 nm. According to F. Ynineb *et al.* [18], this reduction is due to the formation of an amorphous tin phase. Lattice parameters of the deposited films are calculated using the following formula [19]:

$$\frac{1}{d^2_{(hkl)}} = \frac{h^2+k^2}{a^2} + \frac{l^2}{c^2}, \tag{2}$$

$$a = \sqrt{2} d_{(110)}, \tag{3}$$

$$c = \frac{1}{\sqrt{\frac{1}{d_{(hkl)^2}} - \frac{1}{a^2}}}. \tag{4}$$

The crystal defects aroused in films, such as dislocation density δ and micro strain ϵ, of the undoped and indium doped SnO_2 thin films were calculated by the following relations [20, 21] and are depicted in Table I.

$$\delta = \frac{1}{D^2}, \tag{5}$$

$$\epsilon = \frac{\cos(\theta)}{4}. \tag{6}$$

Both the dislocation density δ and the microstrain ϵ show a progressive reduction as the indium content increases up to 15 wt. %, followed by a slight rise at higher doping levels. The initial decline in these parameters reflects a decrease in lattice defects and improved crystalline quality. A similar trend was previously reported by M. Rahaman *et al.*, who examined thickness-dependent structural properties of thermally evaporated In-doped SnO_2 films [20].

The ideal tetragonal SnO_2 lattice constants are $a = 4.74$ Å and c = 3.19 Å [8]. In our study, the undoped film exhibits marginally larger values ($a = 4.750$ Å and c = 3.2019 Å). As indium concentration increases, the c-axis parameter shows a continuous upward shift. In contrast, the a-axis parameter initially decreases to 4.715 Å in the 5-10 wt. % range before rising again to 4.733 Åat 15 wt. % In. This non-monotonic behavior suggests complex lattice accommodation mechanisms involving dopant incorporation and local structural relaxation.

Atomic Force Microscopy (AFM) is among the most effective techniques for probing nanoscale surface features, and it was employed here to analyze the morphology of both undoped and In-doped SnO_2 thin films.

Figure 3 presents the AFM micrographs recorded over a 5×5 μm scan area for samples containing different indium concentrations. All films exhibit smooth, homogeneous surfaces without visible defects that could compromise surface integrity.

The undoped SnO_2 film shows an RMS roughness of 9.6 nm. Upon the incorporation of 5 wt.%, 10wt.%, and 15wt.% indium, the RMS values decrease to 3.7, 4.5, and 4.6 nm, respectively. This reduction in surface roughness indicates that indium plays a significant role in modifying the surface morphology of SnO_2. These observations are consistent with the structural improvements inferred from the XRD analysis.

Figure 4 presents the optical transmission spectra of the In-doped SnO_2 thin films measured over the wavelength interval of 300-900 nm. Independent of dopant concentration, all samples exhibit a high level of transparency across the

TABLE I. The interplanar spacing of the diffraction planes d_{hkl}, RMS, Lattice Parameters (a=b, c), Average Crystallite Size (DXRD), Dislocation Density δ and Microstrain ϵ.

SnO_2/In	d_{hkl} (Å)	RMS	a (Å)	c (Å)	D (nm)	$\delta \times 10^{14}$ cm^{-1}	$\epsilon \times 10^{-3}$
00% In	3.359	9.6	4.750	3.2019	22.8	19.23	15.2
5% In	3.334	3.7	4.715	3.2035	38.9	6.608	8.9
10% In	3.334	4.5	4.715	3.2104	92	1.181	3.75
15% In	3.347	4.9	4.733	3.2104	64.6	2.396	5.36

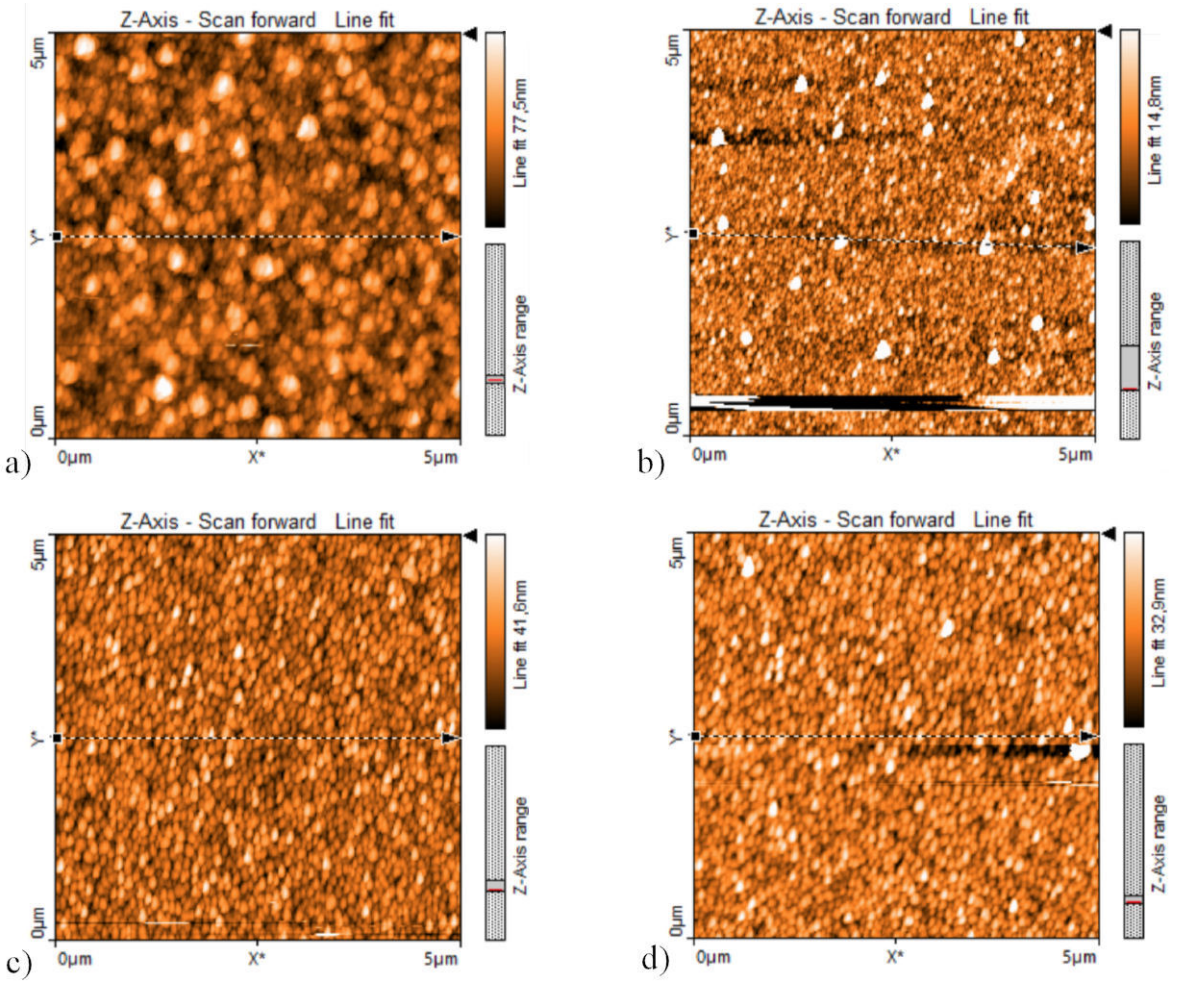

FIGURE 3. AFM images (10 μm $\times$10 μm) of a) SnO2, b) 5wt.% In, c) 10wt.% In, d) 15wt.% In.

visible region, with average transmittance values ranging from approximately 78% to 86%. Such optical behavior confirms that the deposited layers are suitable candidates for applications requiring transparent conducting materials, including thin-film transistors, optoelectronic windows, and photovoltaic devices.

The undoped SnO_2 film demonstrates an average visible-range transmittance of about 82.8%. Introducing 5 wt.% indium results in a noticeable improvement, raising the transmission to nearly 86%, which can be attributed to enhanced film densification and reduced light-scattering centers at low dopant levels. In contrast, further increasing the indium content to 10 wt.% and 15 wt.% induces a slight decline in transparency, with transmission values stabilizing around 79%. This behavior suggests that excessive dopant incorporation introduces additional structural imperfections such as defect states, microstrain, or localized compositional fluctuations that enhance photon scattering and thereby diminish optical clarity.

Comparable observations were reported by S. Sujatha Lekshmy *et al.* [7], who associated the reduction in transmittance at elevated dopant concentrations with scattering

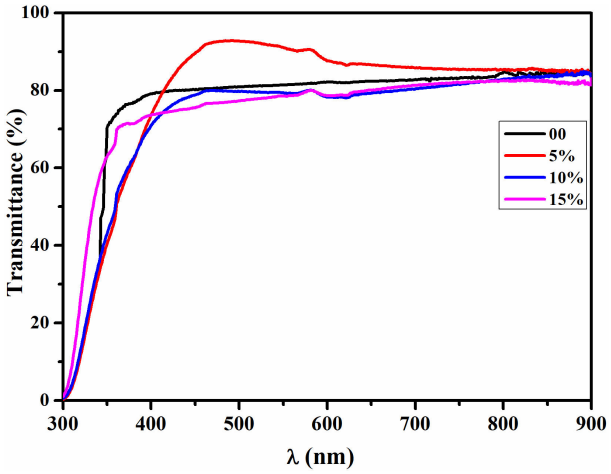

FIGURE 4. UV-Vis spectrum of SnO_2-In with different ratios of In.

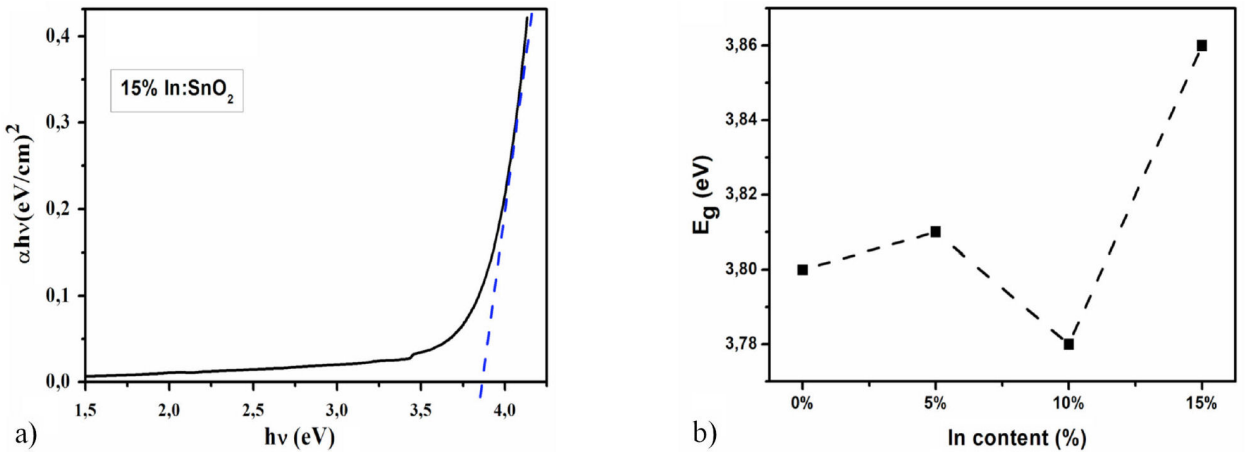

FIGURE 5. a) Example of extrapolation of linear part of $(\alpha h\nu)^2$ versus $h\nu$ plot to $\alpha h\nu = 0$ to determine E_g of 15wt.% In:SnO_2 sample and b) Variation of E_g as function of In content.

phenomena arising from dopant-induced defects within the crystal lattice. The agreement with previous findings reinforces the interpretation that the optical response of SnO_2:In films is strongly governed by the interplay between dopant concentration, structural quality, and defect-mediated light-matter interactions.

The optical band gap was calculated from the Tauc relation [22]:

$$(\alpha h\nu)^2 = \beta(h\nu - E_g). \tag{7}$$

Figure 5 illustrates the evolution of the optical band gap E_g for the undoped and indium-doped SnO_2 (SnO_2:In) thin films. The undoped sample exhibits an experimentally derived band gap of 3.8 eV, which exceeds the nominal bulk value of 3.6 eV [23]. Such a widening of the band gap is commonly associated with size-dependent quantum confinement effects in nanostructured oxide films, as previously documented in the literature [24].

Introducing 5 wt. % indium does not produce any appreciable modification in the optical band gap, suggesting that at low concentrations the incorporated In^{3+} ions do not significantly perturb the electronic structure of SnO_2. When the dopant level is increased to 10 wt.%, a slight reduction of E_g to 3.78 eV is observed. This decrease can be attributed to the formation of additional defect states, such as oxygen vacancies or indium-related donor levels, which introduce localized energy states near the band edges [25]. These states facilitate band-tailing and effectively narrow the optical gap. A comparable phenomenon was reported by B. Thangaraju [26], who associated the band-gap shrinkage in doped SnO_2 films with the emergence of defect-mediated electronic states within the forbidden band.

Upon further increasing the indium concentration to 15 wt.%, the optical band gap expands to approximately 3.86 eV. This recovery and subsequent widening of E_g is consistent with the Burstein-Moss effect [27, 28], wherein heavy doping increases the carrier concentration and shifts the Fermi level into the conduction band. As a result, optical transitions require higher photon energies, producing an apparent blue shift in the absorption edge. This non-monotonic trend reflects the competing influences of defect formation and carrier-induced band-filling on the electronic structure of SnO_2:In thin films.

Figure 6 presents the variation in sheet resistance of the In:SnO_2 thin films as a function of indium concentration, measured at room temperature. The undoped SnO_2 layer exhibits a relatively high sheet resistance of 942 Ω/sq. As the level of In incorporation increases, the sheet resistance decreases markedly, reaching a minimum value of about 104 Ω/sq at 15 wt.% doping. This behavior indicates a strong enhancement in electrical conductivity with increasing dopant content. The reduction in resistance can be explained by the substitution of Sn^{4+} ions with In^{3+} ions in the lattice. Each substitution event introduces an additional free electron, thereby increasing the carrier concentration and promoting n-type conduction, which collectively contribute to the observed decline in sheet resistance [29].

Similar conductivity enhancement mechanisms have been reported in other doped SnO_2 systems. For instance,

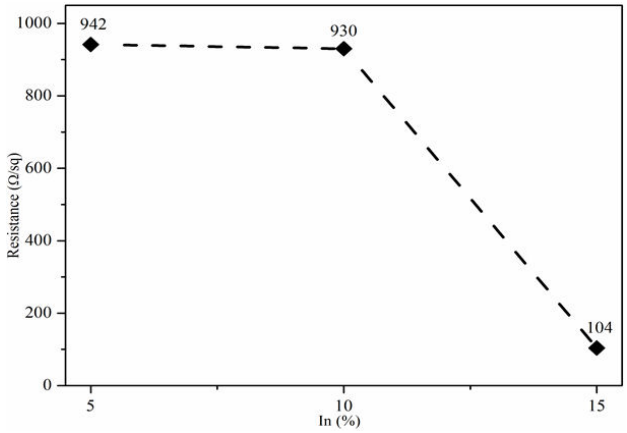

FIGURE 6. Variation of sheet resistance of In:SnO_2 as a function of In content.

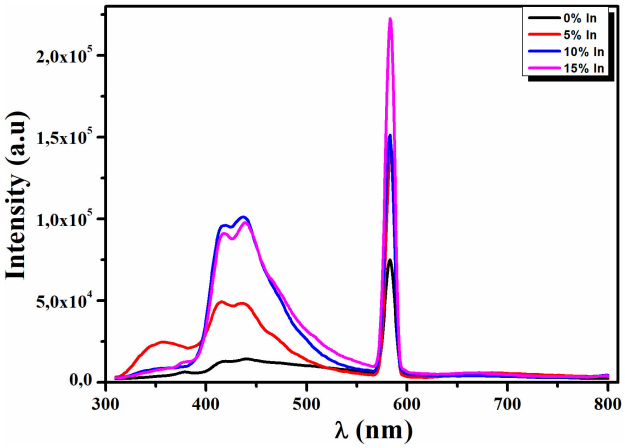

FIGURE 7. Room temperature PL spectra of the undoped and In-doped SnO_2.

Mujdat Caglar *et al.* [30] found that fluorine doping significantly decreased the sheet resistance of SnO_2 films due to the substitution of O^{2-} by F^- ions, which generated extra free electrons. A related study [31] attributed the decrease in sheet resistance at higher indium levels to an increase in hole concentration, highlighting that dopant incorporation can modify the charge carrier population depending on the resulting defect chemistry. These comparisons emphasize that aliovalent doping whether by indium or other species plays a crucial role in tuning the electrical properties of SnO_2 thin films and enhancing their performance as transparent conductive oxides.

One of the most effective non-destructive methods to investigate the optical properties, the specific defects for radiative transitions and impurity levels in the In doped SnO_2 in semiconductor materials is photoluminescence (PL) spectroscopy. Figure 7 displays the room temperature photoluminescence spectra of undoped SnO_2 and in doped SnO_2 from 300 to 800 nm. The pure SnO_2 exhibit an intense peak at 582 nm (2.13 eV), When indium is added to the SnO_2 films, two additional peaks emerge in addition to the first strong one. The first one at 415 nm (2.98) and the second at 439 nm (2.82).

The emission band situated at 582 nm has been linked in the literature to crystalline defects like oxygen vacancies, Sn vacancies, or Sn interstitials, which make up a sizable number of trapped states inside the band gap of SnO_2 nanostructures [32, 33]. The peaks located at 415 nm and 439 nm (a violet emission, 2.98 eV, 2.82 eV) are due to the oxygen vacancies, many authors ascribed the peak situated in the UV-violet range in polycrystalline oxides to oxygen vacancies, which represent the major defects [34, 35].

The overall intensity of PL increases significantly with the doping rate (5% To 15% at. In), the result of increased generation of oxygen vacancies induced by In^{3+}/Sn^{4+} substitution. The higher ionic radius of In^{3+} (80 pm) compared to Sn^{4+} (69 pm) induces lattice distortions, favoring the formation of $V_\circ$ to compensate for charge imbalances according to the reaction:

$$2\mathrm{In}^{3+}\mathrm{SnO}_2 \rightarrow 2\mathrm{In} + V_\circ + \mathrm{O}_2^- . \tag{8}$$

This increase in radiative defect density also broadens the spectral response towards the visible, as evidenced by the effective bandgap reduction observed in highly doped samples. Peaks at 415 nm and 439 nm, absent in pure SnO_2, confirm the catalytic role of indium in defect engineering, aligned with mechanisms reported for other doped metal-based oxides where oxygen vacancies modulate the electronic structure and enhance the efficiency of optical transitions.

Figure 8 illustrates the water droplet profiles formed on undoped and indium-doped SnO_2 thin-film surfaces, from which the water contact angle (WCA) was determined.

All measurements were conducted at room temperature using a 10 μL deionized water droplet. The measured WCAs were 66° for undoped SnO_2 and 35°, 55.3°, and 32° for films doped with 5wt.%, 10wt.%, and 15wt.% indium, respectively. Since all values are below 90°, the deposited films exhibit hydrophilic behavior, with wettability strongly influenced by the indium doping concentration.

A pronounced reduction in the contact angle from 66° to 35° is observed upon 5wt.% indium doping, indicating enhanced surface hydrophilicity. This behavior can be attributed to the reduction in grain size and the associated increase in grain boundary density, which provides additional active sites for water molecule adsorption, thereby increasing surface free energy.

At an indium concentration of 10wt.%, the contact angle increases to 55.3%, which coincides with a significant increase in grain size from 38.9 nm to 92 nm. The enlargement of grains reduces the surface area-to-volume ratio and decreases the density of grain boundaries. Since grain boundaries act as preferential adsorption sites for water molecules, their reduced density leads to a decrease in surface free energy and, consequently, a reduction in hydrophilicity, resulting in a higher contact angle.

With further increase in indium concentration to 15wt.%, the grain size decreases to approximately 64.6 nm, leading to an increase in grain boundary density and surface free energy. This structural modification enhances water adsorption and results in a lower contact angle of 32°, indicating improved hydrophilic behavior.

These observations are consistent with the model proposed by Munshi *et al.*, [27], who demonstrated that contact angle variations are closely correlated with grain size evolution. Smaller grains exhibit a higher surface area-to-volume ratio, which increases surface free energy and leads to lower contact angles, whereas larger grains reduce surface free energy, resulting in increased contact angles.

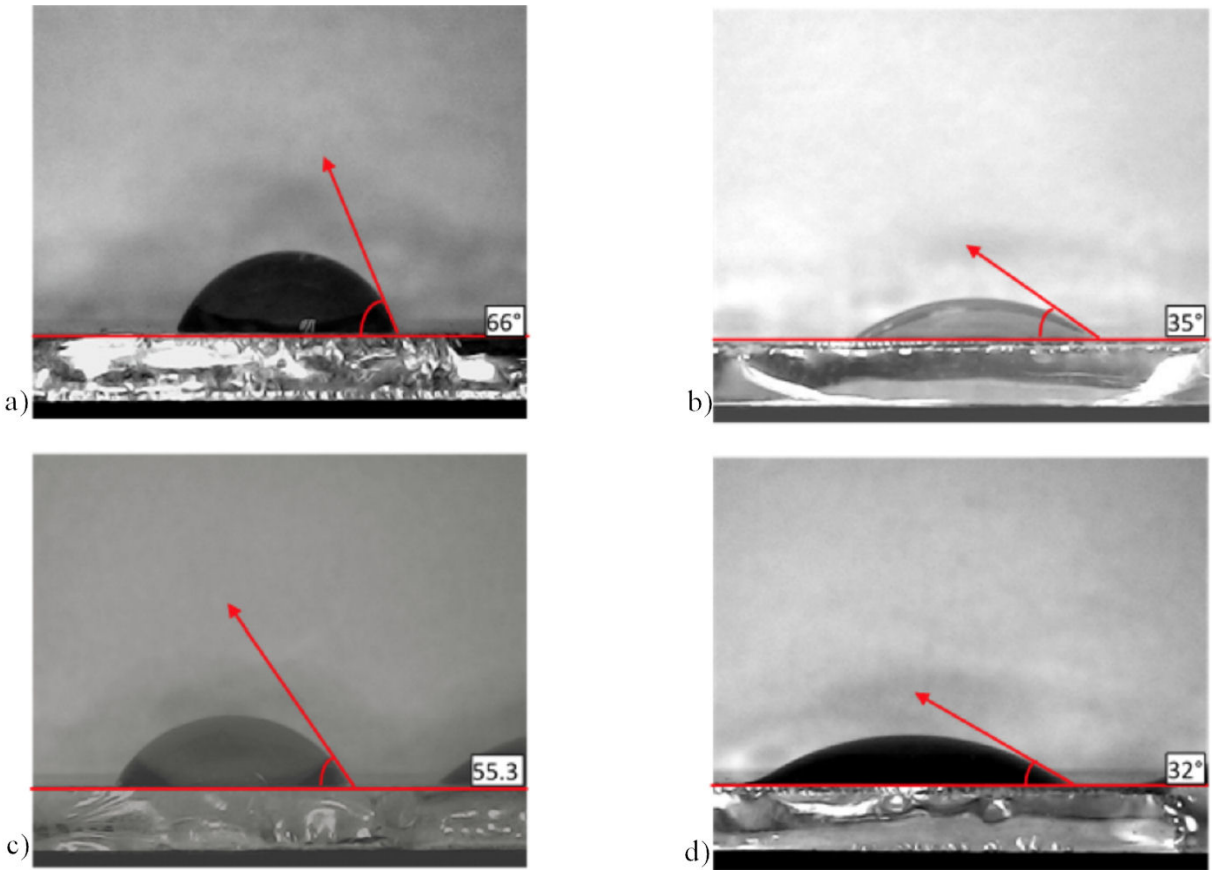

FIGURE 8. Variation contact angle (CA) for undoped and In-doped SnO_2 thin films.

4. Conclusion

In this work, we examined the structural, morphological, optical, electrical, and wettability properties of undoped and indium-doped SnO_2 thin films with In contents ranging from 0 to 15 wt. %. XRD results showed that all films maintained the tetragonal rutile SnO_2 phase with a predominant (110) orientation. Doping with 5 wt. % In enhanced crystallinity and promoted grain growth, while higher dopant levels induced slight peak shifts and mild lattice distortions without generating secondary phases. Grain size increased up to 10 wt. % and then slightly decreased at 15 wt. %, likely due to the formation of amorphous tin-rich regions. AFM confirmed smooth, uniform surfaces across all samples. Optical measurements revealed high visible transmittance (78-86%), with maximum transparency at 5 wt. % doping, while the band gap followed a non-linear evolution, decreasing initially due to defect-related states and subsequently widening at 15 wt. % because of the Burstein-Moss effect.

Electrical analysis demonstrated a substantial decrease in sheet resistance with increasing In content, attributed to improved carrier concentration through In^{3+} substitution at Sn sites. Photoluminescence spectra indicated the growing presence of oxygen vacancies with higher doping levels, acting as radiative recombination centers. Wettability measurements indicate that indium doping induces hydrophilic behavior in SnO_2 thin films, as evidenced by contact angles consistently below $90°$. The observed variation in contact angle with indium concentration is not directly attributable to the indium content itself, but rather to changes in grain size and surface energy. Specifically, the contact angle decreases at an indium concentration of 5 wt.%, increases moderately at 10 wt%, and then decreases again at 15 wt.%.

1. A. Salehi and M. Gholizade, Gas-sensing properties of indium-doped sno2 thin films with variations in indium concentration, *Sensors and Actuators B: Chemical*, **89** (2003) 173.

2. S. Maadadi *et al.*, Investigation of optical, dielectric, and electrical properties of zno/cold sprayed al system and their correlation with photovoltaic performance: S. maadadi et al. *Optical and Quantum Electronics* **57** (2025) 345.

3. W. Ke *et al.*, Low-temperature solution-processed tin oxide as an alternative electron transporting layer for efficient per-

ovskite solar cells, *Journal of the American Chemical Society*, **137** (2015) 6730.

4. P. Liu and V. Sivakov, Tin/tin oxide nanostructures : Formation, application, and atomic and electronic structure peculiarities, *Nanomaterials*, **13** (2023) 2391.
5. A. A. Ahmad, A. Migdadi, and Q. M. Al-Bataineh, Structural, optical, and electrical properties of strontium-doped tin dioxide films for high photoconductivity, *Thin Solid Films*, **796** (2024) 140312.
6. D. Sharma *et al*., Crystal chemistry and physicochemical investigation of aliovalent substituted sno2 nanoparticles, *Vacuum*, **184** (2021) 109925.
7. S. Sujatha Lekshmy and K. Joy, Structural and optoelectronic properties of indium doped sno2 thin films deposited by sol gel technique, *Journal of Materials Science: Materials in Electronics*, **25** (2014) 1664.
8. M. A. Abdulsattar, S. S. Batros, and A. J. Addie, Indium doped sno2 nanostructures preparation and properties supported by dft study, *Superlattices and Microstructures*, **100** (2016) 342.
9. S. Laghrib, M. Benhaliliba, H. Adnani, and D. Abdi, Wide bandgap indium-doped sno2 semiconductor prepared by sol-gel route: Multilayer fabrication and low resistivity for solar cell application, *Journal of Sol-Gel Science and Technology*, **106** (2023) 530.
10. H. Kang, Y. Xiong, L. Ma, T. Yang, and X. Xu, Recent advances in micro-/nanostructure array integrated microfluidic devices for efficient separation of circulating tumor cells, *RSC advances*, **12** (2022) 892.
11. F. Lekoui *et al*., Ag-doped zno nanostructured thin films for transparent antibacterial surfaces: Effect of ag content, *Inorganic Chemistry Communications*, **173** (2025) 113831.
12. B. Cojocaru, D. Avram, V. Kessler, V. Parvulescu, G. Seisenbaeva, and C. Tiseanu, Nanoscale insights into doping behavior, particle size and surface effects in trivalent metal doped sno2, *Scientific reports*, **7** (2017) 9598.
13. Z. Ji, L. Zhao, Z. He, Q. Zhou, and C. Chen, Transparent p-type conducting indium-doped sno2 thin films deposited by spray pyrolysis, *Materials Letters*, **60** (2006) 1387.
14. B. Alemayehu, E. Shin, V. Vasilyev, and G. Subramanyam, Synthesis and characterization of indium-doped sno2-based impedance spectroscopy sensor for real-time humidity sensing applications, *Crystals*, **14** (2024) 82.
15. S. SujathaLekshmy, L. Maneeshya, P. Thomas, and K. Joy, Intense uv photoluminescence emission at room temperature in sno2 thin films, *Indian Journal of Physics*, **87** (2013) 33.
16. A. Hafdallah, F. Ynineb, M. Aida, and N. Attaf, In doped zno thin films, *Journal of Alloys and Compounds*, **509** (2011) 7267.
17. D. Dergham, S. Hassani, F. Lekoui, M. Ouchabane, R. H. Ali, and I. Djemai, Optimisation of optical and electrical properties of zno/au-pd/zno multilayer thin films, in 2022 2nd International Conference on Advanced Electrical Engineering (ICAEE). IEEE, 2022), pp. 1-4.
18. F. Ynineb, A. Hafdallah, N. Attaf, M. S. Aida, J. Bougdira, and H. Rinnert, Microstructure and opto-electrical properties of sno2: In2o3 alloys thin films prepared by ultrasonic spray, *International Journal of Nanoparticles* **11** (2013) 252.
19. B. Teldja, B. Noureddine, B. Azzeddine, and T. Meriem, Effect of indium doping on the uv photoluminescence emission, structural, electrical and optical properties of spin-coating deposited sno2 thin films, *Optik*, **209** (2020) 164586.
20. M. M. Rahaman, K. M. A. Hussain, M. Sharmin, C. Das, and S. Choudhury, Structure, morphology and opto-electrical properties of nanostructured indium doped sno2 thin films deposited by thermal evaporation, *European Scientific Journal, ESJ*, **12** (2016).
21. F. Lekoui *et al*., Elaboration and characterization of pure zno, ag : Zno and ag-fe : Zno thin films : Effect of ag and ag-fe doping on zno physical properties, *Rev. Mex. Fis.* **69** (2023) 0.
22. D. Grine *et al*., Synthesis, characterization, and antibacterial activity of ag-tio2-fe composite thin films, *Physica Status Solidi* (a), **219** (2022) 2200036.
23. M. Okuya, S. Kaneko, K. Hiroshima, I. Yagi, and K. Murakami, Low temperature deposition of sno2 thin films as transparent electrodes by spray pyrolysis of tetra-n-butyltin (iv), *Journal of the European Ceramic Society*, **21** (2001) 2099.
24. W. Zhou, Y. Liu, Y. Yang, and P. Wu, Band gap engineering of sno2 by epitaxial strain : experimental and theoretical investigations, *The Journal of Physical Chemistry C*, **118**, (2014) 6448.
25. F. Lekoui *et al*., Investigation of annealing environment effect on the structural, morphological, and linear/nonlinear optical properties of nanostructured mn-doped zno thin films, *Inorganic Chemistry Communications*, **176** (2025) 114209.
26. B. Thangaraju, Structural and electrical studies on highly conducting spray deposited fluorine and antimony doped sno2 thin films from sncl2 precursor, *Thin solid films*, **402** (2002) 71.
27. A. Munshi, V. Singh, M. Kumar, and J. Singh, Effect of nanoparticle size on sessile droplet contact angle, *Journal of Applied Physics*, **103** (2008) 13.
28. R. Amrani *et al*., Structural and optical properties of highly ag-doped tio2 thin films prepared by flash thermal evaporation, *Physica Scripta*, **99** (2024) 065914.
29. Y. Wang, H. Zhang, X. Zhang, Z. Zhou, and L. Wang, Tuning electrical and optical properties of sno2 thin films by dual-doping al and sb, *Coatings*, **15** (2025) 669.
30. M. Caglar and K. C. Atar, Effect of both deposition temperature and indium doping on the properties of sol-gel dip-coated sno2 films, *Spectrochimica Acta Part A : Molecular and Biomolecular Spectroscopy*, **96** (2012) 882.
31. G. Bhatia, A. D. Acharya, M. Patidar, V. Gupta, S. Shrivastava, and V. Ganesan, Tuning of structural, morphological, optical and electrical properties of sno2 by indium inclusion, *Bulletin of Materials Science*, **44** (2021) 187.
32. R. S. Zeferino, U. Pal, M. E. D. A. Reues, and E. R. Rosas, Indium doping induced defect structure evolution and photocatalytic activity of hydrothermally grown small sno 2 nanoparticles, *Advances in nano research*, **7** (2019) 13.
33. G. Zhou, S. Ni, X. Sun, X. Wang, Q. Wang, and D. He, Visible photoluminescence of hydrothermal synthesized sn1- x ni x o2 nanostructures, *Journal of Materials Science: Materials in Electronics*, **22** (2011) 174.

34. J. Jeong *et al*., Photoluminescence properties of sno2 thin films grown by thermal cvd, *Solid State Communications*, **127** (2003) 595.

35. Y. Du, M.-S. Zhang, J. Hong, Y. Shen, Q. Chen, and Z. Yin, Structural and optical properties of nanophase zinc oxide, *Applied Physics A*, **76** (2003) 171.